Traveling Wave-Like Mesoscale Perturbations in the North Pacific Current

WARREN B. WHITE

Scripps Institution of Oceanography, University of California, San Diego, La Jolla, CA 92093

(Manuscript received 22 July 1981, in final form 15 October 1981)

ABSTRACT

Individual seasonal mean maps of temperature at 300 m in the North Pacific Current east of 180° from 1976 to 1980 were constructed from TRANSPAC XBT data. The long-term annual mean map is relatively smooth, with some weak quasi-stationary meander activity. Most of the total variance was due to large-scale interannual variability (i.e., ~60%), less to the mesoscale perturbations (i.e., ~30%), and least to the annual cycle (i.e., ~10%). However, individual mesoscale perturbations were significant, clearly wave-like with a wavelength scale of 500–1000 km and a period scale of 1–2 years, and generally coherent in phase over 10° of latitude. These wave-like mesoscale perturbations emanated from the eastern boundary and propagated westward as coherent features at the phase speed of linear, non-dispersive, baroclinic long-waves. The latitudinal reduction in phase speed from 2.7 cm s^{-1} at 35°N to 1.4 cm s^{-1} at 45°N was consistent with baroclinic long-wave theory. An increase in time scale of these wave-like perturbations with latitude was consistent with the "critical latitude" concept.

1. Introduction

Bernstein and White (1977) conducted a study of mesoscale variance in the main thermocline of the midlatitude North Pacific, finding the western region populated by "large" mesoscale perturbations and the eastern region populated by "small" ones, with variance much less by an order of magnitude. In a more recent study, Bernstein and White (1981), using TRANSPAC XBT (expendable bathythermograph) data collected routinely over the western midlatitude North Pacific each month, investigated the stationary and transient mesoscale perturbations in the Kuroshio extension. In the present study, mesoscale perturbations in the eastern region (Fig. 1) are investigated. From the map of surface dynamic height in Fig. 1, this latter region (enclosed in heavy lines) is historically the location of the broad sluggish flow of the North Pacific Current.

This study is made possible by routine collection of XBT observations by the TRANSPAC volunteer observing ships (VOS) program. Examples of the monthly data distribution from this program are shown in Fig. 2. Originally, the TRANSPAC VOS XBT program (White and Bernstein, 1979) was not designed to detect mesoscale perturbations in the thermal field of the eastern region, only large-scale, climate-related, temperature residuals. In fact, in earlier studies (e.g., White *et al.*, 1980) the mesoscale perturbations were treated as sub-grid ambient noise contaminating the measure of the large-scale features. However, as analyses progressed, it became clear that mesoscale features were more persistent than had been previously supposed.

Bernstein and White (1974) conducted a study of mesoscale perturbations using a wide variety of historical data sources. In the eastern North Pacific between 20 and 30°N, they found mesoscale perturbations with a correlation space scale of 100–200 km, associated with a correlation time scale of 3–4 months. Dorman and Saur (1978) extended this type of analysis farther north, from 20 to 40°N, using XBT data collected monthly between San Francisco and Honolulu. They reported similar correlation scales (i.e., 200 km space scale, 3-month time scale). Bernstein and White (1977) computed mesoscale wavenumber spectra in the eastern region from early TRANSPAC XBT data, finding the mean spectrum to have peaked near wavelengths of 800 km (i.e., corresponding to a correlation length scale again of 200 km).

More information concerning time and space scales of mesoscale perturbations in the eastern region comes from inspection of trajectories of satellite-tracked drifting buoys (McNally, 1981). Numbers of drifting buoys, drogued at 30 m depth and deployed in the eastern mid-latitude North Pacific during the summers of both 1976 and 1977, became trapped in 100 km eddy-like features, circulating around and around in nearly the same location for up to three months. Other drifting buoys, streaming to the east, traced out mesoscale perturbations of up to 1000 km in wavelength, again nearly frozen in space for up to three months.

0022-3670/82/030231-13$07.25

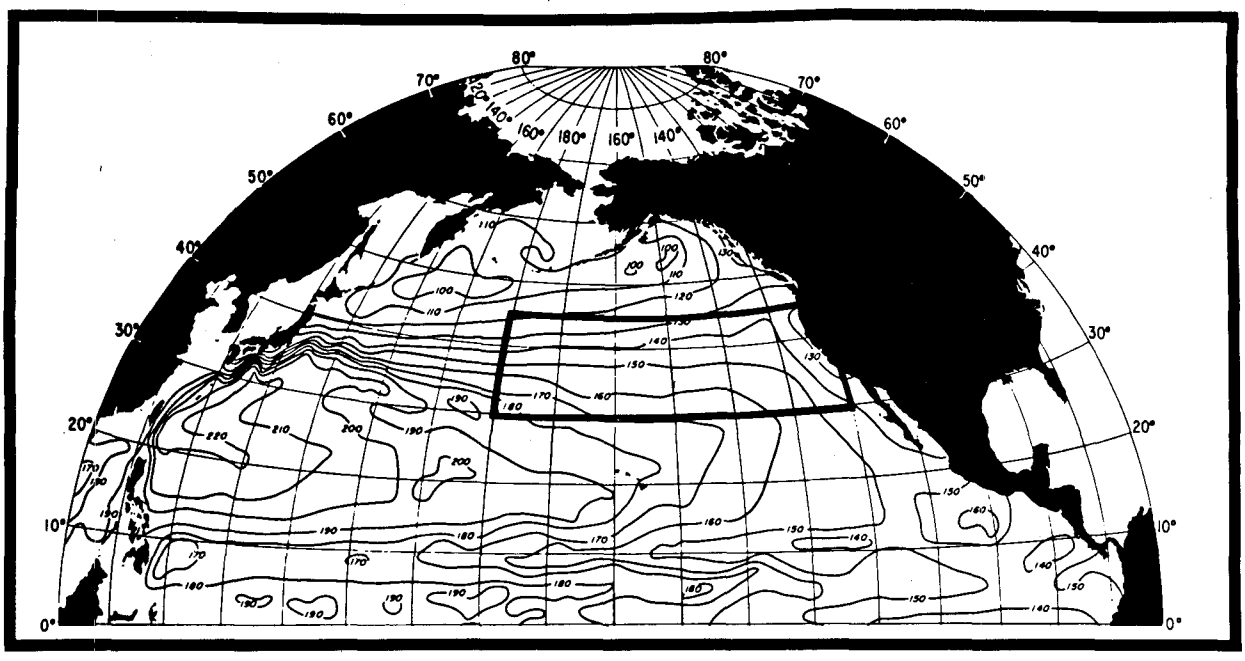

FIG. 1. Dynamic topography of the sea surface (0/1000 db) produced by Wyrtki (1975) for the mid-latitude North Pacific, with the region of interest outlined.

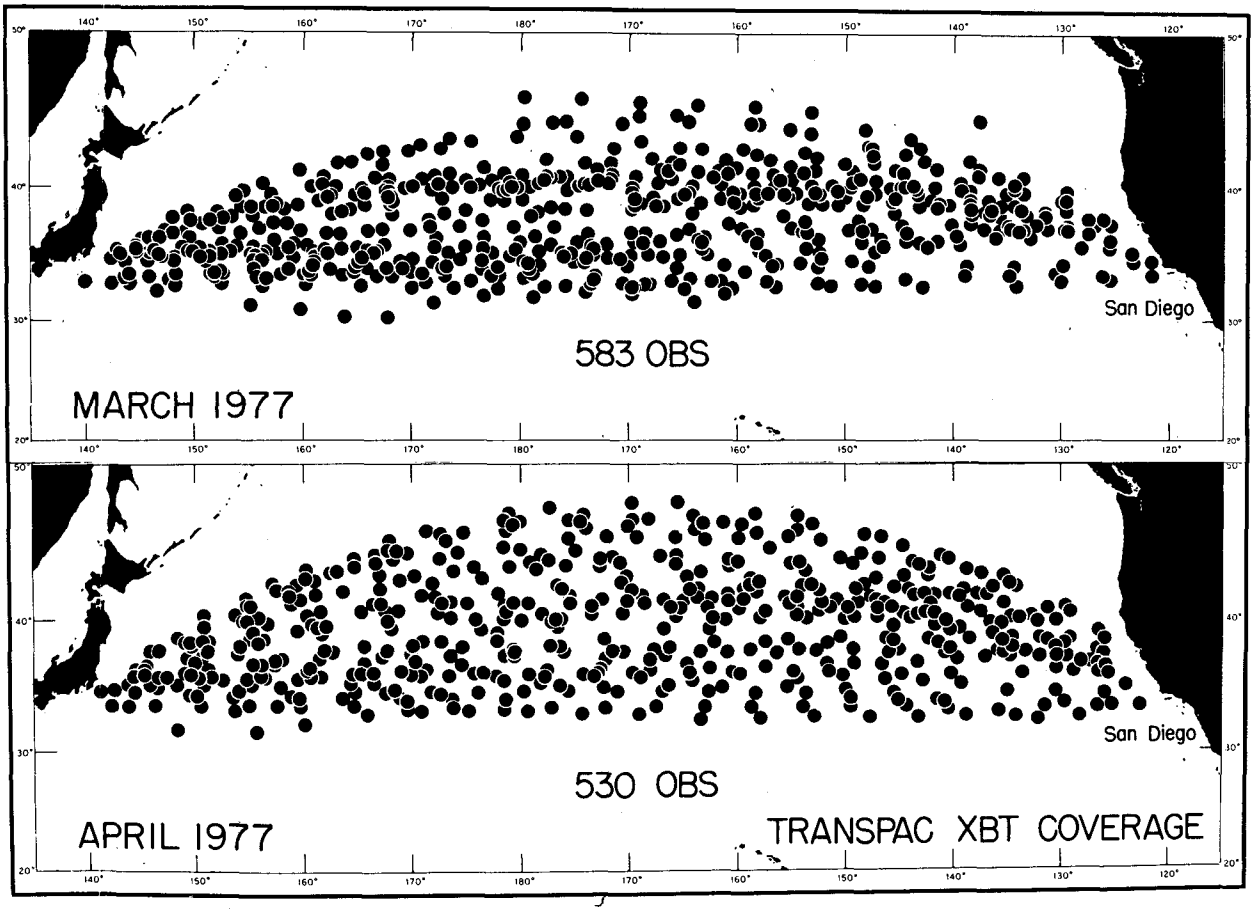

FIG. 2. Distribution of XBT observations for two months, April and May 1977, taken by the TRANSPAC volunteer observing ships (VOS) XBT program.

Based upon these foregoing studies, mesoscale perturbations in the eastern midlatitude North Pacific can be considered to have a typical wavelength scale of from 500–1000 km and a typical time-period scale of one year or more. In order to resolve these perturbations in the main thermocline, individual seasonal mean maps of temperature at 300 m depth over the entire eastern midlatitude region (Fig. 1) have been constructed for four years beginning in summer of 1976. While this time resolution was marginally adequate to resolve mesoscale perturbations of one year period, it was more than adequate to resolve those of two-year period. In partial compensation for the lack of temporal resolution, the increased spatial data density in these seasonal maps (i.e., combining three months of XBT data of the kind of distribution shown in Fig. 2) allowed for 1° latitude × 1° longitude resolution over much of the map even after smoothing. This was more than adequate to observe 500 km wavelength perturbations.

2. Initial mapping results

Seasonal maps of temperature at 300 m were constructed over the eastern region using linear trend analysis (i.e., Surface II) developed at the University of Kansas (Sampson, 1973). Individual temperature observations were interpolated to a 0.5° latitude × 0.5° longitude grid, first by fitting a trend surface to the nearest eight surrounding observations, and then selecting the value at the grid point from this surface. This interpolation procedure smoothed the data field, but this effect was limited by employing a maximum search radius for observations of 3° latitude/longitude. Further smoothing was employed prior to contouring, removing 2-grid noise. Hence, resolution of each map was 1° latitude × 1° longitude but the ability to detect perturbations of this scale depends primarily upon the local data density. Therefore, the locations of XBT observations are included on each map. Contouring of the gridded field was done objectively by Surface II.

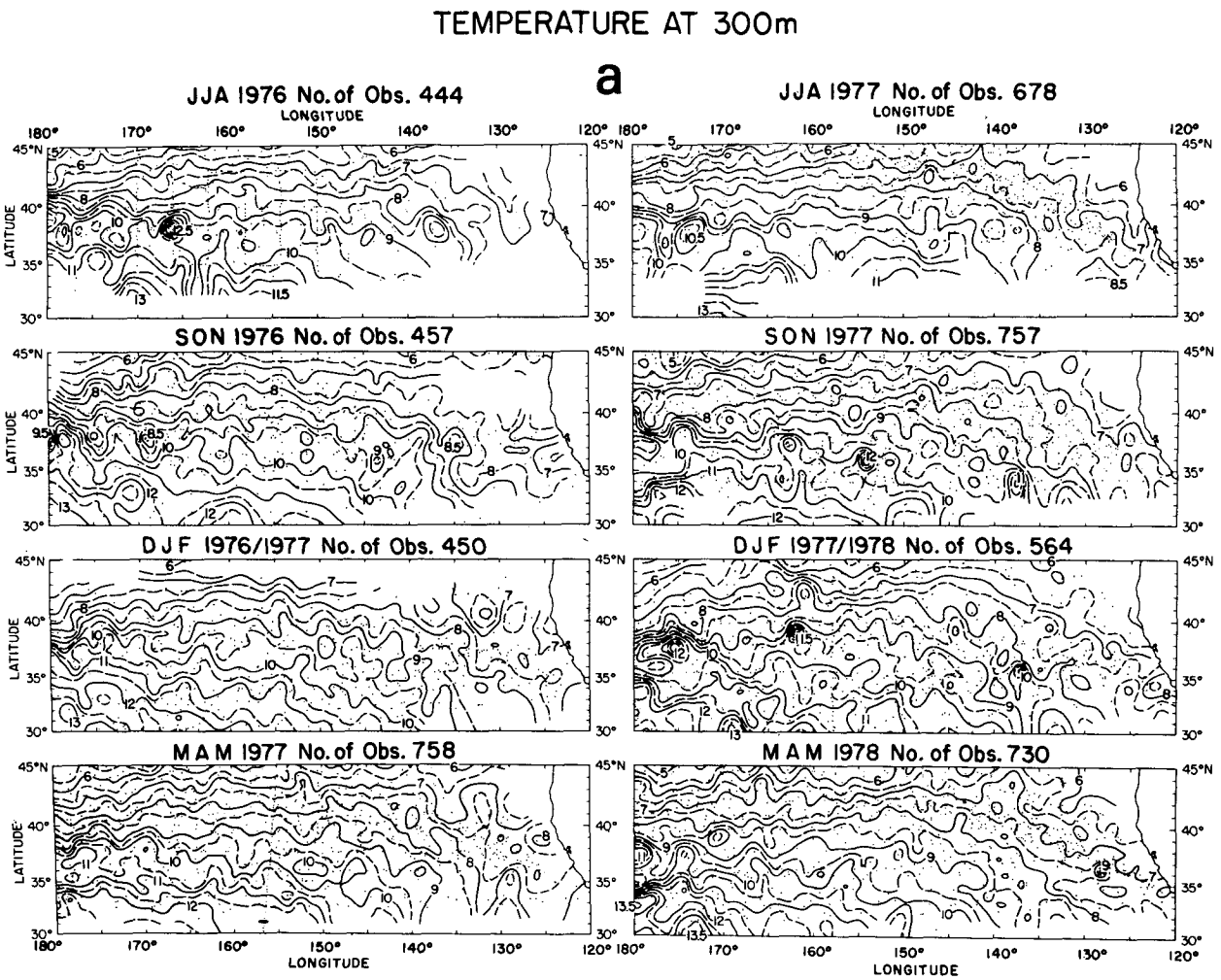

FIG. 3. Individual seasonal mean maps of temperature at 300 m over the region of interest, from (a) summer 1976 to spring 1978 and (b) summer 1978 to spring 1980. The small dots represent locations of individual XBT observations.

This interpolation scheme did not provide an estimate of interpolation error. However, a conservative estimate can be made from statistics compiled during earlier studies of the TRANSPAC-XBT data set. White and Bernstein (1979) reported that a conservative estimate of the instrumental error in the XBT observation itself (including thermistor error and drop-rate error) was no larger than 0.1°C. Bernstein and White (1977) found that scales of motion of <100 km, acting here in the same way as instrumental error, had a standard deviation no more than ±0.15°C. Therefore, the standard deviation of the total noise (sub-grid noise plus instrumental noise) in the present study can be considered to have been no more than ±0.18°C. With smoothing, both during the interpolation procedure and afterwards, the error in the interpolated value can conservatively be put at ±0.06°C. As will be shown, this measure of error is smaller than the contour interval needed to resolve the mesoscale perturbations.

Resulting seasonal maps are displayed in Figs. 3a and b, extending from the summer of 1976 to the spring of 1980. The contour interval was 0.5°C, much larger than the estimated interpolation error. On each map, locations of the individual XBT observations were displayed with small dots. Overall data density increased each year of the TRANSPAC VOS program, beginning in the summer of 1976 with a total of 444 observations for the eastern region and ending in the spring of 1980 with 956 observations. There was some spatial bias in the data distributions, with summer data concentrated more along the great circle route between North America and Japan and with winter data concentrated more along the rhumb line. In these areas, resolution is truly 1° latitude/longitude; away from these regions it may be more, depending upon the local data density.

In the interior portion of the mapped region can be seen ubiquitous wave-like mesoscale perturbations, with typical wavelength of 5–10° of longitude

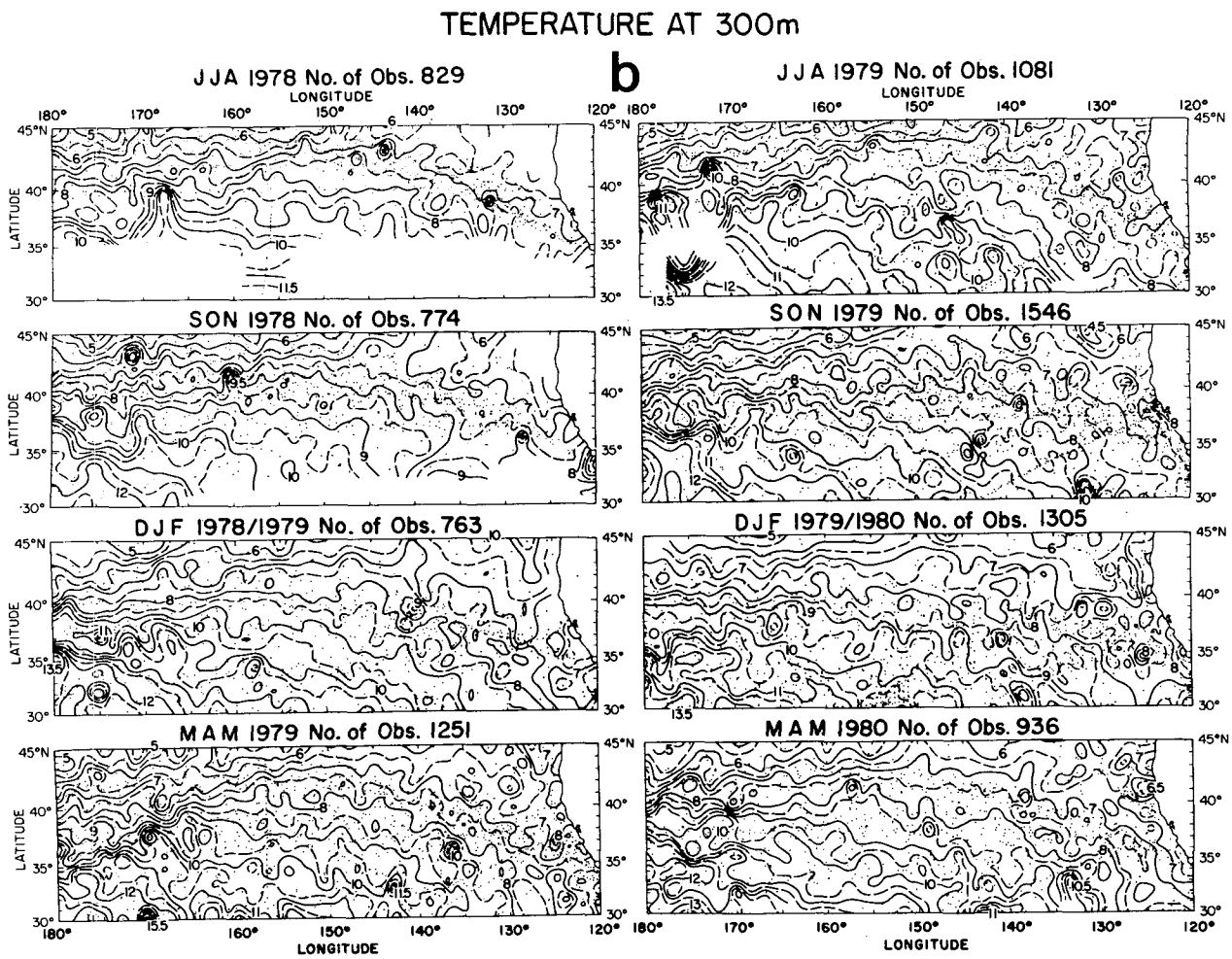

FIG. 3. (*Continued*)

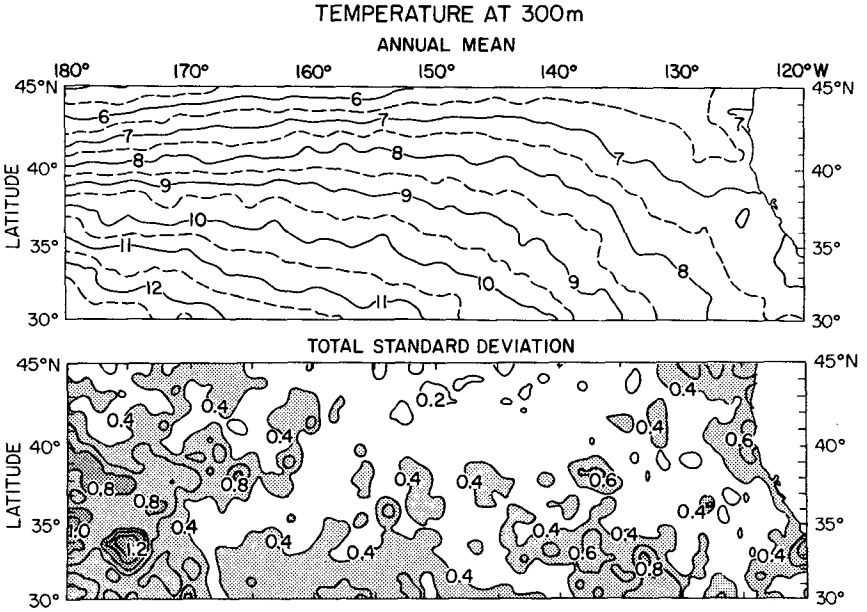

FIG. 4. Annual long-term mean and total standard deviation of temperature at 300 m from summer 1976 to spring 1980.

and meridional isotherm displacement of 1–2° of latitude. Meridional coherence of these wave-like perturbations was surprisingly large, in some cases exceeding 10° of latitude. This is indicative of the presence of long-crested wave activity, discussed in more detail later.

The scale of mesoscale perturbations in each map was relatively independent of data density. For example, those in autumn (September, October, November) of 1976, each resolved with over 25 data points, had roughly the same scale as those in winter (December, January, February) of 1976–77, each resolved with only five data points.

In addition to wave-like mesoscale perturbations, there appeared in these maps closed eddies or rings, most of which seem to exist south of 40°N. In the western part of the region, between the Kuroshio Extension Current at 36°N and the Subarctic Front at 40°N, was a region heavily populated by both cyclonic and anticyclonic rings. Further upstream near Japan, Kawai (1979) has documented the actual evolution of these rings, but their presence this far to the east had not been observed previously. Quite a lot of ring activity was found in the vicinity of the eastern boundary, particularly in the latter 1.5 years (i.e., 1979–1980) when data density there increased. Coastal processes have for some time been known to accelerate this kind of activity (e.g., Bernstein *et al.*, 1977; Stumpf and Legeckis, 1977; Willmott and Mysak, 1980).

Resolution of rings seen in these maps was not as good as wave-like mesoscale perturbations, since the former were so much smaller (i.e., 50 km correlation scale) than the latter (i.e., 200 km scale). Moreover, some rings may have been artificial, associated with large, undetectable, temperature errors in raw XBT data. As such, this study will exclude discussion of rings, concentrating attention on the larger wave-like mesoscale perturbations.

3. Annual mean and standard deviation

From temperature information contained in Fig. 3, the annual long-term mean and total standard deviation for the four years was calculated and mapped in Fig. 4. Resolution in these maps is 1° latitude × 1° longitude, with an accuracy in the mean (i.e., standard error) that can be estimated by dividing the total standard deviation by 4.

The annual mean map of temperature at 300 m has the same general pattern as the annual mean dynamic height map of Wyrtki (1975) shown in Fig. 1, but does of course show more detail. In the western portion of the region, the Subarctic Front at 40°N extended eastward in a gentle arc that took it to 42°N at 155°W, thereafter losing its character as a coherent frontal feature. Another strong frontal feature in the western portion of the region near 36°N was a manifestation of the Kuroshio Extension Current (Bernstein and White, 1981). This current extended eastward to near 170°W, thereafter losing its intense character as a coherent eastward shear flow. Within this short segment of intense eastward shear flow were a number of quasi-stationary mean-

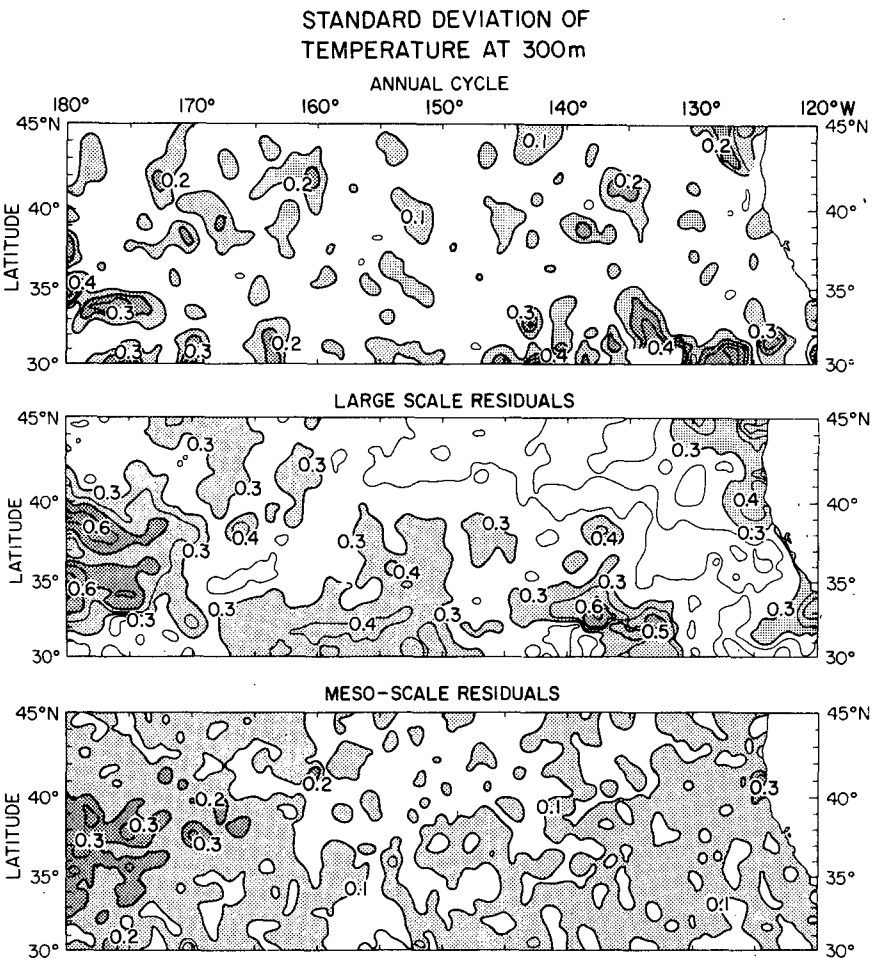

FIG. 5. Standard deviation of temperature at 300 m for the annual cycle, for the large-scale climate-related residuals, and for the mesoscale residuals. See text for further explanation.

ders that displayed meridional coherence of up to 5° of latitude.

The spatial pattern of the total standard deviation is remarkably similar to that of baroclinic potential energy (0/500 db) produced by White (1977a) from his analysis of the historical hydrographic data base. The magnitude was large in the west, where intense eastward shear flows of the Subarctic Front and the Kuroshio Extension Current were found; they were weak in the central portion of the region north of 35°N; and they were large again in the eastern boundary region. Within this general context, the detail is patchy and, aside from the obvious relationship with the mean shear flow in the western portion of the region, is not easy to interpret.

In subsequent analysis, concentration is upon mesoscale wave-like perturbations observed in Fig. 3. Therefore, both the annual cycle and the large-scale, climate-related, variability must be separated from the mesoscale variability. Description of this procedure will be given in the next section. In this section, however, the standard deviation associated with these three different kinds of variability are mapped in Fig. 5. This allows for a comparison of the relative importance of each to the overall variance.

The large-scale standard deviation was in general 2–3 times the mesoscale standard deviation, the latter 1–2 times the standard deviation of the annual cycle. Amplitude of the annual cycle was probably underestimated, since it was based only on seasonal mean values, but its magnitude and what little spatial pattern existed is consistent with a similar map produced by White (1978) in an analysis of historical XBT data collected in this region from 1968–74. Because large-scale variance so dominated the others, its spatial pattern of standard deviation was very similar to that of the total, discussed earlier in Fig. 4.

The spatial pattern of the mesoscale standard deviation was in general quite homogeneous, except in the high shear flow region of both the Kuroshio Extension Current at 36°N and the Subarctic Front at

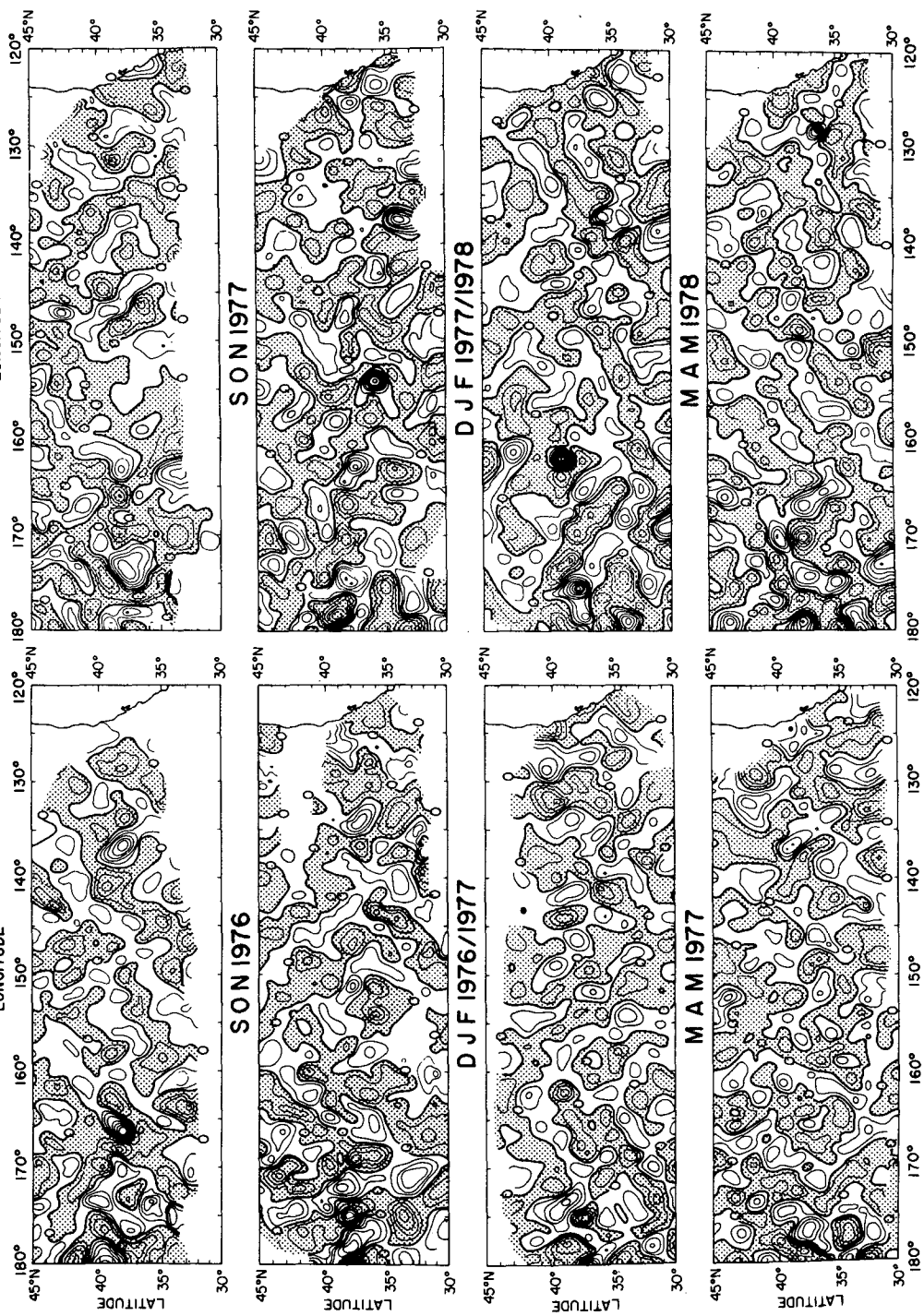

FIG. 6. Individual seasonal mean maps of mesoscale residual temperature at 300 m over the region of interest, from (a) summer 1976 to spring 1978 and (b) summer 1978 to spring 1980. These maps are high-passed versions of those found in Figs. 3a and 3b with contour intervals of 0.1°C. See text for further explanation.

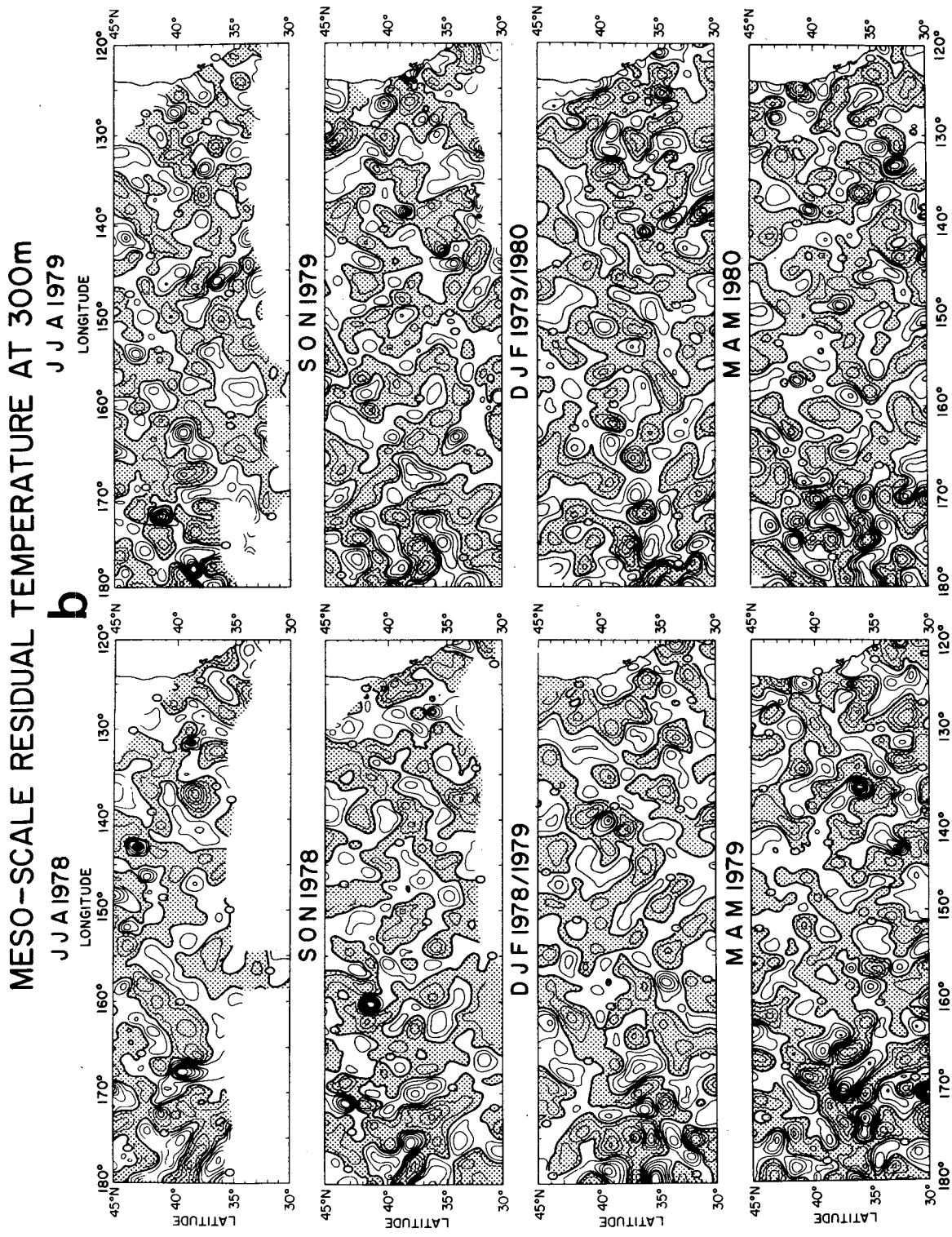

FIG. 6. (*Continued*)

40°N. East of this there was some weak tendency for mesoscale standard deviation to have been largest at the eastern boundary, diminishing to the west. This westward attenuation extended farther to the west with decreasing latitude.

4. Maps of mesoscale residual temperature

Initial seasonal maps of 300 m temperature in Fig. 3 have been highpass filtered to produce mesoscale maps, shown in Fig. 6a and b. The procedure for producing these maps is simple but effective. First, 1° latitude × 1° longitude interpolated data used to construct the maps in Fig. 3 were transformed into residuals by subtracting the annual cycle. Standard deviation of this annual cycle was mapped in Fig. 5. Next, these residual values were operated upon with a 2° latitude × 5° longitude running mean, producing "large-scale" residual maps on a 1° latitude × 1° longitude grid. This 2° × 5° running mean is similar to that used by White and Bernstein (1979) in their resolution of large-scale, climate-related, temperature residuals. It was chosen on the basis of anisotropy in the large-scale temperature residual field, which finds the zonal scale ~2 times larger than the meridional scale. Standard deviation of this large-scale residual variability over the entire four year period was mapped in Fig. 5. Finally, large-scale residual values were subtracted from the original set of residuals, producing a set of "mesoscale" residual maps. These mesoscale maps are thereby constrained to smaller wavelength scales in the north–south direction (i.e., <4° latitude) than in the east–west direction (i.e., <10° latitude). This is expected to enhance the detection of baroclinic long waves in the midlatitude North Pacific (Kang and Magaard, 1980). These maps were contoured objectively by Surface II, with a 0.1°C contour interval. Standard deviation of this mesoscale residual variability over the entire four-year period was mapped in Fig. 5.

With the mean annual cycle, and large-scale residual variability removed, resultant individual seasonal mesoscale maps in Fig. 6 clearly display the long-crested wave-like nature of the mesoscale perturbations. In the region east of 155°W, wave crests generally aligned themselves in the northeast–southwest direction (e.g., Dec–Jan–Feb 1977–78; March–April–May 1978). Fewer examples can be found showing crests aligned meridionally (e.g., March–April–May 1977) or in the northwest–southeast direction (e.g., Sep–Oct–Nov 1976). In the region west of 155°W, relatively persistent direction of alignment was absent, with as many examples of northeast–southwest alignments as the opposite. Still, quasi-meridional character continued to persist. In the vicinity of the Kuroshio Extension Current and the Subarctic Front west of 170°W, much more in the way of isolated ring activity is to be noted.

5. Westward propagation of mesoscale perturbations

Wave-like mesoscale perturbations seen in Fig. 6 had a persistence from map to map that was difficult to see in that type of display. However, this persistence can be convincingly demonstrated when data from these maps are used to construct time–longitude matrices. In Fig. 7 three such matrices are shown, each extending along constant latitude (i.e., 35, 40, 45°N) from 120 to 180°W and extending in time from summer 1976 to spring 1980.

At each latitude in Fig. 7, season-to-season persistence was clearly evident, with positive and negative mesoscale residuals propagating westward as coherent features throughout the entire four years of record. At 40 and 45°N, where data coverage extended to the coast of North America, *mesoscale perturbations originated at the coast.* Based upon this, those residuals farther away from the coast may have originated at the coast before the beginning of this record.

Quantitative estimates of the speed of this westward propagation can be made by constructing a correlation matrix from each of the time–distance matrices in Fig. 7. These correlation matrices, shown in Fig. 8, also yield information on correlation zonal space and time scales of variability.

The most basic result of this correlation analysis was the speed of westward propagation, increasing from a value of 1.4 cm s^{-1} at 45°N to 2.7 cm s^{-1} at 35°N. Moreover, the time scale of variability decreased from 45 to 35°N. At 45°N it was 6 months (i.e., 2-year period scale) while at 35°N it was 3 months (i.e., 1-year period scale). These latter waves are the random phase, annual, baroclinic Rossby waves discussed by Kang and Magaard (1980).

The magnitude of westward phase speed and its decrease with latitude was consistent with baroclinic long-wave theory (White, 1977b). The equation for these waves, expressing a balance between planetary vorticity and divergence of the water column, is written as

$$-\frac{f^2}{g'H_0}V_t + \beta V_x = 0, \tag{5.1}$$

where V is the meridional velocity of the upper layer of a two-layer system (with lower layer considered at rest); β is the meridional derivative of the Coriolis parameter f; g' is reduced gravity of the upper layer; and H_0 is mean thickness of the upper layer.

The phase speed for natural waves of this system can be written

$$C_x = \frac{-\beta g'H_0}{f^2}. \tag{5.2}$$

Using the same values of parameters in (5.2) as those used by White and Saur (1981) in their study of

annual baroclinic long waves (i.e., $\beta = 2 \times 10^{-13}$ cm^{-1} s^{-1}, $g' = 3$ cm s^{-2}, $H_0 = 250$ m), the phase speed C_x in (5.2) is calculated as a function of latitude and displayed in Fig. 9, together with observed values taken from the correlograms shown in Fig. 8. Basic agreement between theory and the observed westward propagation of mesoscale perturbations is easily seen.

This discovery of wave-like mesoscale perturbations, traveling westward with period scales from 1–

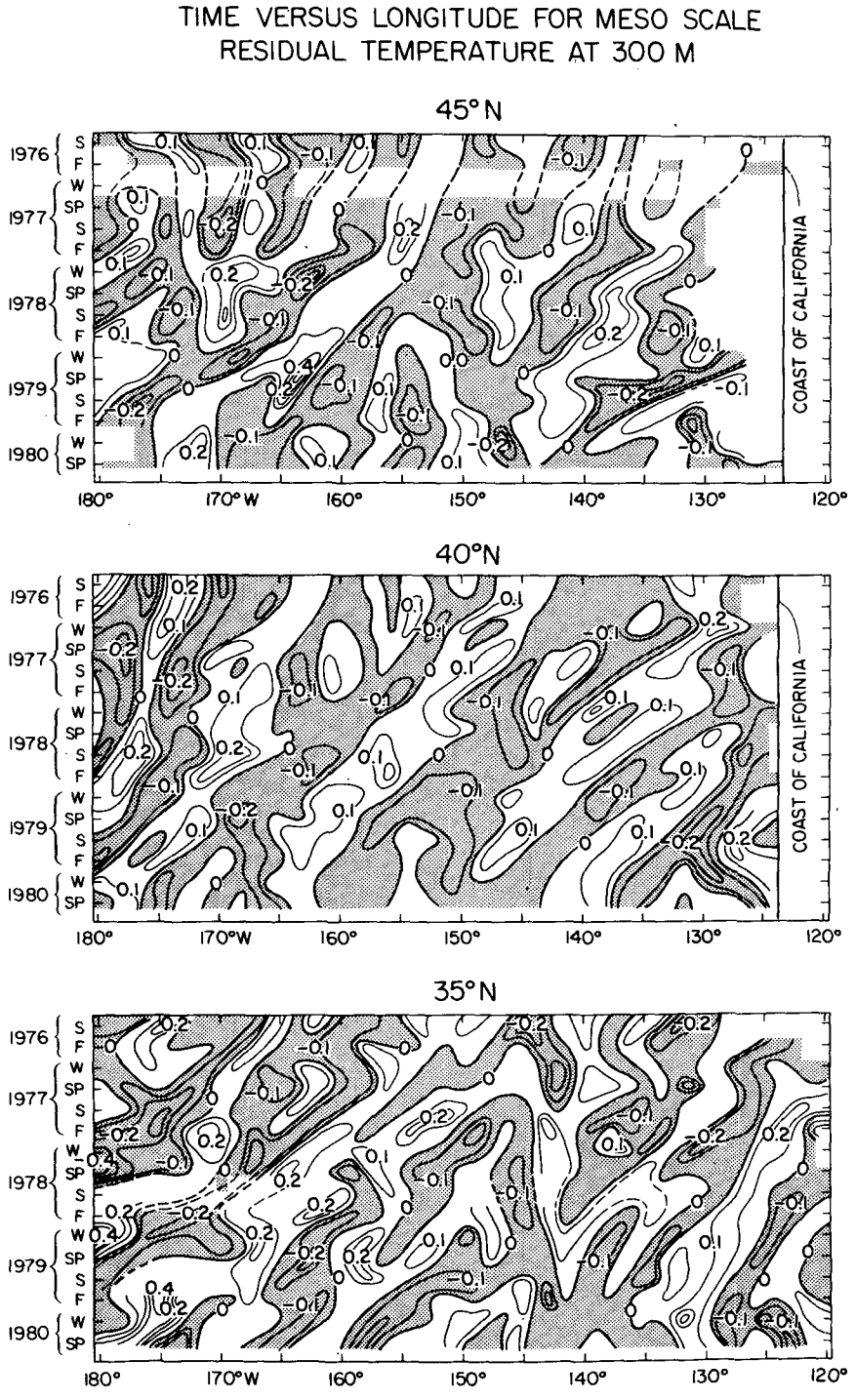

FIG. 7. Time–longitude plot of mesoscale residual temperature at 300 m at 45, 40, and 35°N. Data are the same as used in the construction of Figs. 6a and b.

2 years at speeds that conform to baroclinic long wave theory is not new. Kang and Magaard (1980) had already demonstrated the existence of these wave-like features by fitting (with least squares estimation procedures) a Rossby-wave model spectrum to sample spectra computed from these same TRANSPAC-XBT data. However, their methodology did not produce an actual mapping of these wave-like perturbations, as is shown in Figs. 5 and 6, nor did it allow the individual mesoscale perturbations to be traced westward as coherent features from their source either at or near the eastern boundary. On the other hand, their work, by virtue of its spectral context, has the benefit of statistical rigor that is lacking in this study.

6. Increase in time scale with latitude

Comparison in Fig. 9 shows good agreement between theory and observation. The decrease in phase speed with latitude explains the tendency of wave-like mesoscale perturbations in Fig. 6 to have been aligned in the northeast–southwest direction, the result of refraction effects discussed already by White (1977b). At each latitude, the zonal length scale was approximately the same (i.e., ~600 km), but the time scale increased with latitude, accounting for the decrease in phase speed. The simple model by White (1977b) does not explain the increase in time scale with latitude. This is because model Eq. (5.1) is a simplification of a more general model that takes into account the concept of critical latitude. The critical latitude restricts waves of shorter period from propagating westward away from the eastern boundary at higher latitude.

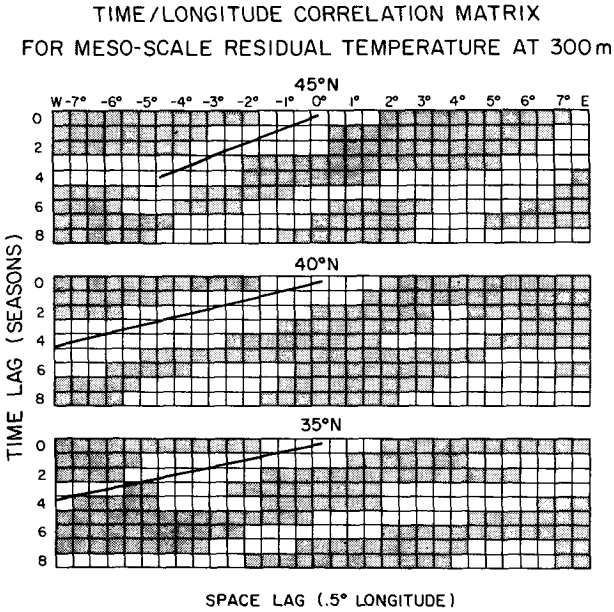

FIG. 8. Time–longitude correlation matrix for mesoscale residual temperature at 300 m for 45, 40 and 35°N. White area indicates positive correlation and black area negative correlation.

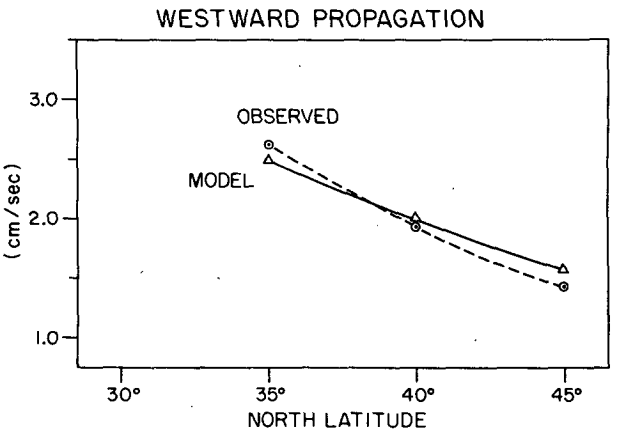

FIG. 9. Plot of zonal phase speed as a function of latitude, from observed data and from a two-layer baroclinic long-wave model.

The model Eq. (5.1) is adequate at latitudes where the zonal scale of motion L is much larger than the Rossby radius of deformation [i.e., $L \gg (g'H_0/f^2)^{1/2}$]. At mid-latitude, L may be on the same order of the Rossby radius of deformation; therefore, the following model equation applies:

$$V_{xxt} - \frac{f^2}{g'H_0} V_t + \beta V_x = 0. \qquad (6.1)$$

This equation differs from (5.1) by inclusion of the relative vorticity term (V_{xxt}) which makes natural waves of the system take on dispersive character.

The dispersion relation for the model expressed in (6.1) can be written in the form

$$k = -\frac{\beta}{2}\omega\left[1 \pm \left(1 - \frac{4\omega^2}{\beta^2}\frac{f^2}{g'H_0}\right)^{1/2}\right], \qquad (6.2)$$

where ω is the frequency of the wave. When the radicand in (6.2) is zero, a critical latitude (θ_{cr}) can be defined through f, beyond which zonally propagating waves of a certain frequency are trapped near the eastern boundary (i.e., the wave amplitude decreases exponentially to the west). The critical latitude has the following analytical expression

$$\theta_{cr} = \tan^{-1}\left[\frac{(g'H_0)^{1/2}}{2R\omega}\right], \qquad (6.3)$$

where R is the radius of the earth. Note that for longer periods ($2\pi/\omega$), the critical latitude is greater.

The question now is two-fold. First, can the critical latitude concept explain why there was a restriction on shorter time-scale variability at higher latitudes? Second, if so, can the mesoscale perturbations that did exist at a particular latitude be shown to have

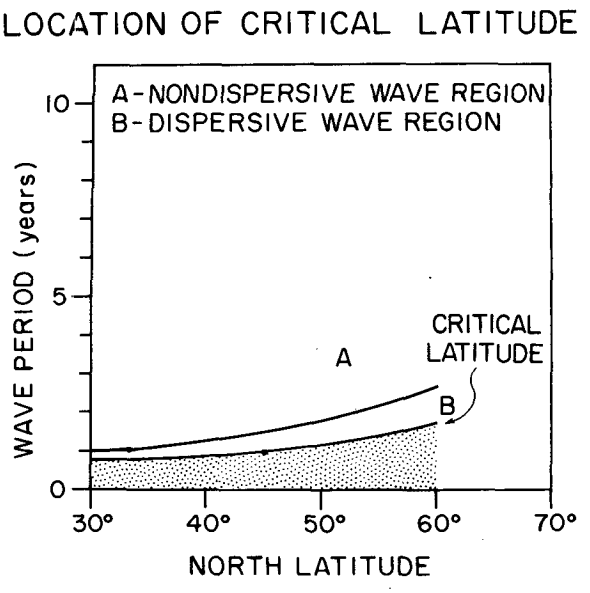

FIG. 10. Plot of critical latitude and latitude separating the dispersive wave region (B) from the non-dispersive wave region (A). See text for further explanation.

obeyed the dispersion relation (5.2) as an approximation to (6.2)?

For conceptual reasons, three separate latitude regions need definition. Poleward of the critical latitude, baroclinic waves of a particular period are trapped locally. Hence, in this region no traveling perturbations emanate from or near the eastern boundary. Equatorward, but near the critical latitude, waves with the same period have a dispersive phase speed that can be determined from (6.2). Hence, in this region traveling perturbations can emanate from the eastern boundary but they disperse as they travel westward. Equatorward of this latter region, waves with the same period have a non-dispersive phase speed determined from (5.2). In this region, westward-traveling perturbations would not disperse and would be expected to be seen as coherent features at locations far from the eastern boundary.

The critical latitude θ_{cr} is plotted against period in Fig. 10, using the same values of g' and H_0 as in the construction of Fig. 9. From this plot, the critical latitude is 45°N for a period of one year, 63°N for a period of two years, and 71°N for a period of three years. Since 60°N is the northern limit of the North Pacific Ocean, all perturbations exceeding a two-year period scale are theoretically not locally trapped anywhere along the eastern boundary.

Since the critical latitude for baroclinic perturbations of a one-year period scale or more is 45°N (i.e., the northern limit of the present study), it remains to determine at what latitude those perturbations can be considered composed of non-dispersive waves. This is estimated by determining at what latitude a wave of period T propagates a zonal distance L that is $\sqrt{10}(2\pi)$ times the Rossby radius of deformation. When L is this large, the magnitude of the term V_{xxt} in (6.1) is an order of magnitude smaller than the term $(g'H_0/f^2)V_t$, and so to a good approximation (6.1) reduces to (5.1).

The plot of this curve is also shown in Fig. 10, separating region A, where non-dispersive waves can occur, from region B where they cannot and where allowable waves take on a dispersive character. For a period scale of one year, baroclinic perturbations can be non-dispersive south of 33°N. For a period scale of two years, this latitude is 52°N and for waves of a three-year period, all baroclinic perturbations in the North Pacific basin can be non-dispersive. Dispersive character can set in for perturbations with sufficiently short meridional scales.

Of course, these results are subject to changes if the value of the internal gravity wave speed [i.e., $(g'H_0)^{1/2}$] is taken differently. Moreover, it ignores the spatial and temporal changes in this quantity over the North Pacific basin. It also ignores meridional changes in phase. For this reason, a more accurate discussion of this subject requires usage of more realistic numerical models. What can be shown here is a certain measure of consistency between observations and theory.

In terms of the foregoing discussion, the fact that wave-like mesoscale perturbations increased in time scale with increasing latitude is understood to be consistent with the more general baroclinic wave theory. Recall that, in Fig. 8, the dominant period scale at 35°N was one year, while at 45°N it was two years. Moreover, these waves were non-dispersive (i.e., in Fig. 7 individual perturbations were persistent over the entire four years) appearing to have emanated from the eastern boundary. The disappearance of these nondispersive waves of one-year period north of 40°N is consistent with the concept of a poleward limit (i.e., critical latitude) to the non-dispersive waves of the same period.

The theory predicts that waves of one-year period in this region would be dispersive and so would be poorly resolved by this data set. The fact that the wave-like mesoscale perturbations had a zonal length scale that was constant with latitude, results from the application of the spatial filter to the original mapped data, which fixed the dominant zonal spatial scale in the mesoscale maps to between 500 and 1000 km at all latitudes. Of course, if no critical latitude existed, and if waves were non-dispersive at all frequencies at all latitudes, then the spatial filter would be an effective time filter as well, in which case waves of one-year period would be restricted south of 40° N.

7. Conclusion

Similarities and differences exist between the character of wave-like mesoscale perturbations in the

western midlatitude North Pacific (Bernstein and White, 1981) and those reported in this study.

In both regions, the standard deviation of wave-like mesoscale perturbations had a magnitude that was directly related to that in mean shear flow of the Kuroshio Extension Current (i.e., west of 170°W). However, east of 170°W this current diminished radically in strength and the mesoscale standard deviations found in the North Pacific Current were nearly uniform over the entire region, with some slight increase approaching the eastern boundary. As such, a tentative distinction can be made between those wave-like mesoscale perturbations associated with the Kuroshio Extension Current and those found in the vicinity of the North Pacific Current east of there.

Despite an apparent dynamical difference between wave-like mesoscale perturbations in the eastern and western mid-latitude North Pacific, their correlation scales were on the same order (i.e., 125–250 km, 3–6 months, respectively). Moreover, in both regions, the wave-like mesoscale perturbations propagated westward. However, a significant discrepancy existed in the speed of propagation. In the western region, Bernstein and White (1981) observed an average speed at 37°N of -4 cm s^{-1}, nearly twice the theoretical linear wave speed. In the present study, the observed wave speed in the eastern region was found to conform to the theoretical linear wave speed (i.e., -2 cm s^{-1} at 37°N), even to the point of agreeing with its latitudinal variation.

While it can be stated that the source of the mesoscale wave-like perturbations in the Kuroshio Extension Current remains unknown, there is mounting evidence that wave-like mesoscale perturbations in the North Pacific Current were baroclinic long waves generated at or near the eastern boundary. These perturbations originated at the coast and traveled westward as coherent non-dispersive features, in agreement with theory. Moreover, the fact that these perturbations decreased in time scale with latitude is consistent with the critical latitude concept of the theory. It remains now to seek the source mechanism for the generation of these perturbations.

Acknowledgments. This study arose from many discussions with Gerry McNally, whose drifting buoy analyses first suggested the existence of nearly frozen waves and meanders in the North Pacific Current. The map construction was made possible by the efforts of Ted Walker, who, as computer programmer was instrumental in their subsequent analysis.

This research was sponsored by the Office of Naval Research under ONR Contract N00014-75-C-0152 and by the University of California, San Diego, Scripps Institution of Oceanography.

REFERENCES

Bernstein, R., and W. White, 1974: Time and length scales of baroclinic eddies in the central North Pacific Ocean. *J. Phys. Oceanogr.*, **4,** 613–624.

——, and ——, 1977: Zonal variability in the distribution of eddy energy in the mid-latitude North Pacific Ocean. *J. Phys. Oceanogr.*, **7,** 123–126.

——, and ——, 1981: Stationary and traveling mesoscale perturbations in the Kuroshio Extension Current. *J. Phys. Oceanogr.*, **11,** 692–704.

——, L. Breaker and R. Whritner, 1977: California Current eddy formation: ship, air, and satellite results. *Science*, **195,** 353–359.

Dorman, C., and J. F. T. Saur, 1978: Temperature anomalies between San Francisco and Honolulu 1966–1974, gridded by objective analysis. *J. Phys. Oceanogr.*, **8,** 247–257.

Kang, Y., and L. Magaard, 1980: Annual baroclinic waves in the central North Pacific. *J. Phys. Oceanogr.*, **10,** 1159–1167.

Kawai, H., 1979: Rings south of the Kuroshio. *The Kuroshio IV*, Saikon Publishing Company, 250–273.

McNally, G., 1981: Satellite tracked drift buoy observations of the near surface flow in the eastern mid-latitude North Pacific. *J. Geophys. Res.*, **86,** 8022–8030.

Sampson, R., 1973: Users manual for SURFACE II graphics system. Kansas Geological Survey, University of Kansas, 144 pp.

Stumpf, H., and R. Legeckis, 1977: Satellite observations of mesoscale eddy dynamics in the eastern tropical ocean. *J. Phys. Oceanogr.*, **7,** 648–658.

White, W. B., 1977a: Secular variability in the baroclinic structure of the interior North Pacific from 1950–1970. *J. Mar. Res.*, **35,** 587–607.

——, 1977b: Annual forcing of baroclinic long waves in the tropical North Pacific Ocean. *J. Phys. Oceanogr.*, **7,** 50–61.

——, 1978: A wind-driven model experiment of the seasonal cycle of the main thermocline in the interior mid-latitude North Pacific. *J. Phys. Oceanogr.*, **8,** 818–824.

——, and R. Bernstein, 1979: Design of an oceanographic network in the mid-latitude North Pacific. *J. Phys. Oceanogr.*, **9,** 592–606.

——, R. Bernstein, G. McNally, S. Pazan and R. Dickson, 1980: The thermocline response to transient atmospheric forcing in the interior North Pacific 1976–1978. *J. Phys. Oceanogr.*, **10,** 372–384.

Willmott, A., and L. Mysak, 1980: Atmospherically forced eddies in the northeast Pacific. *J. Phys. Oceanogr.*, **10,** 1769–1791.

Wyrtki, K., 1975: Fluctuations in the dynamic topography in the Pacific Ocean. *J. Phys. Oceanogr.*, **5,** 450–459.